Journal of Building Engineering 67 (2023) 106004

Contents lists available at ScienceDirect

Journal of Building Engineering

journal homepage: www.elsevier.com/locate/jobe

Damping evaluation of an eight-story steel building with nonlinear oil damper under strong earthquakes

Yunjia Tong [a], Songtao Xue [a,b], Liyu Xie [a,*], Hesheng Tang [a]

[a] Dept. of Disaster Mitigation for Structures, Tongji University, Shanghai, 200092, China
[b] Dept. of Architecture, Tohoku Institute of Technology, Sendai, 982-8577, Japan

ARTICLE INFO

Keywords:
Damping identification
Steel building
Nonlinear oil damper
Fluid viscous damper Kelvin-Voigt model
Particle filtering
Parameter identification supplemental damping estimation
Strong earthquake

ABSTRACT

Fluid viscous damper has been applied widely for energy dissipation and shock absorption in dynamic structural systems, specifically the oil damper. Nevertheless, there's an issue of precisely incorporating shaft bearings and pressure sealings for oil dampers, which restricts its wide application in new or existing structures. A type of nonlinear oil damper with viscoelastic polymer packing soft links is posed and investigated to allow for easy production. To explore the effectivity and actual performance of the nonlinear oil dampers, vibration monitoring system has been instrumented both on the dampers and the building since it was built in 2003, which accumulated huge amount of precious data. A Bayesian based order selection of auto-regressive exogenous model is exploited to the recorded earthquake responses to extract dynamic properties of the passively-controlled 8-story steel building. Thus, damping characteristics of the whole structure can be identified and analyzed. Besides, an analytical model for the nonlinear oil damper is investigated and estimated by particle filter improved with Metropolis-Hastings algorithm, which can be incorporated into the whole structure model for model updating, reliability as well as response prediction. Furthermore, the calculation formulas of the additional effective damping ratio provided by oil damper are deduced based on above analysis using modal strain energy, and damping ratio of the main steel frame structure are also estimated. Taking a set of actual ground motion monitoring data as an example, the proposed method is then exploited to estimate the effective damping ratio of oil damper for each floor.

1. Introduction

Vibration control plays a vital role in civil engineering, especially for tall buildings or structures constructed in earthquake-prone area, which may experience substantial vibration due to wind or earthquake. Under severe earthquakes, vibration incurs massive forces, acceleration and displacement to structural and nonstructural elements, which turns the building uncomfortable to live on top, barely able to function normally, highly unstable or even collapse eventually. In order to dissipate the vibration energy input to buildings as possible, multiple vibration control approaches have been designed and posed to address this difficulty during the past 50 years, especially consisting of active, semi-active, and passive control devices [1].

Since 1970s, the passive structural control methods have been utilized extensively to suppress structural chatter in earthquake engineering. Because implementation and operation of passive control apparatuses are relatively simple and robust without requirements for actuators, outside power supplies and sensors [2]. As the supplemental passive damping apparatuses are able to

* Corresponding author.
E-mail address: liyuxie@tongji.edu.cn (L. Xie).

https://doi.org/10.1016/j.jobe.2023.106004
Received 24 October 2022; Received in revised form 29 January 2023; Accepted 29 January 2023
Available online 31 January 2023

considerably improve the vibrational performance of structures through absorbing and dissipating most of the input energy, which other than be absorbed by lateral load resisting system of the building. Thus, the forced chatter, displacement, acceleration as well as inelastic deformation of the structure go down significantly [3].

Passive control apparatuses in civil engineering mainly include hysteretic dampers, friction dampers, velocity-dependent dampers (e.g. viscous fluid dampers and viscoelastic dampers), and tuned mass dampers, etc. [4–7]. They are generally considered effective and reliable to mitigate hazards posed by wind and earthquake as well as rehabilitate deteriorating structures. According to the Japan Society of Seismic Isolation, there are more than 7000 buildings equipped with seismic isolators or supplemental damping devices in Japan [8]. Many research works have been done on experimental investigation (full-scale or small-scale) of passive control apparatuses to examine or evaluate dynamic characteristics and mathematical models of passive control apparatuses [9–18]. However, actual performance of most passively-controlled buildings has seldom been tested by real earthquakes. Besides, the actual performance of the passive control devices during major and catastrophic earthquakes has barely been tested, since the frame members of structures remained mostly elastic during the shaking table tests.

Fluid viscous damper (FVD) is one kind of additional passive damping apparatuses that have been well-established and used extensively in new and retrofit constructions in recent years [19–29]. In general, fluid viscous damper consists of a cylinder and a piston, and the cylinder is divided by the piston into two compartments, which are filled with viscous liquid such as oil, then usually referred to as oil damper. Nevertheless, one challenge with oil damper is that their demand of machining precision is extremely strict, thus, the cost is relatively expensive. To address this difficulty, a type of nonlinear oil damper is propounded with a gap between cylinder and piston to allow for easy production, which is then packed with viscoelastic polymer [30]. In this research, the oil dampers of this type are implemented on an eight-story steel building serving as passive energy absorbing apparatuses. In order to further explore the effectivity of the nonlinear oil dampers and actual performance of the eight-story steel building with nonlinear oil damper under strong earthquakes, structural health monitoring system has been instrumented on both the steel building and the oil dampers to evaluate their long-term behaviors, states as well as damping, since it was built in 2003, which cumulated huge amount of precious data.

Based on the response monitoring data of the eight-story steel building with nonlinear oil damper under strong earthquakes, an auto-regressive exogenous (ARX) model method is employed to extract dynamic properties of the whole steel building. Since the model order selection was critical and nontrivial for successfully identifying the inherent damping characteristic of the building. Bayesian technique was then introduced to decide the order of ARX models based on inferring the posterior probability of ARX models with various model orders [31–33]. Finally, a Bayesian based order selection of auto-regressive exogenous model is exploited to the recorded earthquake responses to extract dynamic properties of the eight-story steel building with nonlinear oil damper. Thus, damping characteristics of the whole structure can be identified and analyzed.

Besides, in order to evaluate the damping contribution offered by nonlinear oil dampers, mathematical model which can capture the primary dynamic properties of the nonlinear oil dampers is crucial for being incorporated into structural computational models, for successful application in design practice, as well as for model updating and response prediction. Maxwell model has been used extensively to represent the traditional linear oil damper. Nevertheless, the nonlinear oil damper in this research is significantly different from traditional linear oil damper, since it also generates viscoelastic resisting force by shear motion of sealing rings except the resisting force from inner pressure differential of fluid when oil flows through orifice. The dynamic behaviors of the nonlinear oil damper been studied experimentally in small-scale [52,53], which mainly focus on the implementation of the nonlinear oil damper to mitigate seismic vibration of structure. With the progress of the nonlinear oil dampers from theoretical designs into practical applications, reliable methods for model identification are necessary to assess if the damper is working as designed and validate the expected performance.

(a) (b)

Fig. 1. The building: (a) Front elevation; (b) Detailed distribution of oil dampers and accelerometers (blue square represents damper, red dot represents load cell and red triangle represents accelerometers). (For interpretation of the references to colour in this figure legend, the reader is referred to the Web version of this article.)

Among various nonlinear identification methods, particle filtering approach is capable of dealing with any distribution even non-Gaussian, which estimates the posterior density distribution merely using a group of random samples from that density. Therefore, an analytical model of the nonlinear oil damper is then identified with model uncertainties quantified by the particle filter algorithm improved with Metropolis-Hastings [34–36]. The identified model and posterior distribution of unknown parameters demonstrate that the improved particle filtering approach can be appropriately used for nonlinear parameter identification without stuck to special particles. Furthermore, based on above analysis, the calculation formulas of the additional effective damping ratio provided by oil damper are deduced using modal strain energy, and damping ratio of the main steel frame structure are also estimated. Taking a set of actual ground motion monitoring data as an example, the proposed method is then exploited to estimate the effective damping ratio of oil damper for each floor.

2. Building description

2.1. Structural system

This research aims to explore the performance of an eight-story Administration Building on the pronounced campus of the Tohoku Institute of Technology (Fig. 1 (a)) located in Sendai. The main lateral load resisting system of the building is provided by braced steel frames of the structural system. The dimension of the main building is 48 m long, 9.6 m wide, and 34.2 m high, with 10 bays in longitudinal direction and three bays in transverse direction, as shown in Fig. 1 (b). The load resisting system of the superstructure is composed of precast concrete slabs working with braced steel frames, and the one-story basement is composed of reinforced concrete. This steel building itself was designed according to Japanese Earthquake Resistance Code for School Buildings even without considering any control devices. In order to verify the effectiveness of a newly developed oil damper and improve the structural earthquake resistance capability, 56 sets of dampers were installed in the building, which were distributed evenly on each floor with four sets of oil dampers in each direction, that is, total eight sets of oil dampers for every floor. The Oil dampers incorporate with the V-type steel braces to execute energy dissipating work, which are installed between the adjacent floors, as illustrated in Fig. 1 (b). Two sets of oil damper specifications with respect to different stroke limits and orifice shape specifications are designed for 1st floor (Type I) and 3rd to 8th floor (Type II), respectively. The nominal first floor and second floor from the structural view are integrated to constitute a large space with a height of 8 m [37].

2.2. Instrumentation

The structural and vibration monitoring systems have been set up on the building since the building was constructed in 2003, which are mainly made up of 4 triaxial accelerometers (3 accelerometers placed on carefully selected story of the building and 1 accelerometer on the ground near the building). Servo-type accelerometers were allocated on the first, fourth, eighth floors. At the same time, the displacement-meters and strain gauges were deployed to gauge the inter-story drifts, axial displacements and axial damper forces of damper braces. Small servo accelerometer CV-374AV(A) with a specific specification, of which has a resolution of 0.01 cm/s^2 and measurement range of ± 2000 cm/s^2, were selected to record floor acceleration responses. All the sensors are linked together through local area network, and the clock built in each sensor is precisely synchronized with both Global Position System (GPS) and Network Time Protocol (NTP) server. Once the threshold ground acceleration of 0.5 cm/s^2 is transcended, the trigger will activate the monitoring system to record seismic responses of the building. The sampling frequency of recorded seismic responses were 200 Hz and 100 Hz for earthquake events before 2011 and after 2012. Moreover, the seismic response recordings were stored in a server for further analysis. Note that horizontal accelerations were oriented in east–west (EW) and north–south (NS) directions corresponding to longitudinal and transverse directions of the building.

3. System identification using ARX models

In this paper, system identification analysis of recorded seismic responses of the building are presented. The paper mainly focuses on the analysis of recordings of large earthquakes. Therefore, recorded data with respect to four large earthquake records with a moment magnitude more than 7.0 are employed for analysis. The detailed basic information about the four large earthquakes are displayed in Table 1 as follows.

Among them, a recorded data set of a large earthquake with a moment magnitude of 7.0 on 26th May 2003 (called 'Record20030526 data' hereinafter) was analyzed as an example. Because the recorded seismic motion has non-flat distribution in frequency domain, the time-domain auto-regressive exogenous (ARX) model methodology was adopted to analyze the recorded data of the building.

The ARX model is a time-series model in a discrete time domain, which can be derived from dynamic equilibrium equation of

Table 1
Information of earthquakes.

Date	Time	Location		Epicentral distance	Depth	Magnitude
(y/m/d)	(UTC)	N (∘) E (∘)		(km)	(km)	M
2003/5/26	9:24:33	38.849	141.568	88.6	68	7
2005/8/16	2:46:28	38.276	142.039	102.1	36	7.2
2011/3/9	2:45:20	38.435	142.842	173	32	7.3
2011/4/7	14:32:43	38.276	141.588	62.7	42	7.1

structural system [38]. The coefficient matrices of ARX model are able to construct the system matrix of structure, and then the eigenvalue decomposition of the system matrix can be used to estimate the dynamic properties of the structure. In general, least square method is employed to estimate the coefficient matrices of the ARX model [39–43]. However, selecting an appropriate order for ARX model is difficult. Although Akaike's Information Criterion (AIC) can be utilized for the model order selection, it does not always select a reasonable model order in practice especially when the order of model is large. Stabilization diagram method has also been proposed to determine the order of the ARX model, whereas, it belongs to empirical criteria and does not have strong theoretical foundations. Therefore, Bayes' Theorem is applied to decide order of ARX models based on the well-established Bayesian probabilistic framework [31,44–47].

3.1. ARX model and Bayesian techniques

3.1.1. ARX model and Bayesian model selection

In general, the mathematical equation of ARX model can be expressed as follows:

$$A(q)y(t) = B(q)u(t) + w(t) \tag{1}$$

in which t denotes the discrete time, y and u are the output and input of the system, respectively, and w is assumed to be Gaussian white noise, which is used to sculpture the model error and uncertainty(generally include non-parametric model errors, noise in measured inputs, and unmeasured inputs). $A(q)$ and $B(q)$ denote the polynomial functions of autoregressive coefficients {ai}, {bi}, and are defined as follows:

$$A(q) = 1 + a_1 q^{-1} + \cdots + a_{n_a} q^{-n_a} = 1 + \sum_{j=1}^{n_a} a_j q^{-j} \tag{2}$$

$$B(q) = b_1 q^{-n_k} + \cdots + b_{n_b} q^{-n_b+1-n_k} = \sum_{j=1}^{n_b} b_j q^{-j+1-n_k} \tag{3}$$

in which q^{-1} is assigned as a backward move operator, namely, $q^{-1}y_k = y_{k-1}$, n_a and n_b are orders of the output and input of the system, respectively. n_k denotes the delay in time domain, Then, equation (1) can be revised as follows:

$$y_k = -\sum_{j=1}^{n_a} a_j y_{k-j} + \sum_{j=1}^{n_b} b_j x_{k-j+1-n_k} + w_k = \psi_k \theta + w_k \tag{4}$$

$$\psi_k = \left[-y_{k-1} \cdots -y_{k-n_a} \;\; u_{k-n_k} \cdots u_{k-n_k-n_b+1} \right] \tag{5}$$

$$\theta = \left[a_1 \cdots a_{n_a} \;\; b_1 \cdots b_{n_b} \right]^{\mathrm{T}} \tag{6}$$

where θ is defined as an autoregressive coefficient vector, and ψ describes a vector integrating both the output and input.

Consider σ^2 is the variance of prediction error and also an unknown parameter of the model, thus, the autoregressive coefficient vector is redrafted to be $\theta_e = [\theta^{\mathrm{T}} \; \sigma^2]^{\mathrm{T}}$. Moreover, the revised parameter vector is capable of determining the whole model of the system for an ARX model class $\mathscr{U}(n_a, n_b, n_k)$. Based on recorded data $\mathscr{D} = \{u, y\}$ and Bayes' Theorem, the posterior probability density (PDF) function of parameter vector θ_e is given by:

$$p(\theta_e | \mathscr{D}, \mathscr{U}) = \frac{p(\mathscr{D} | \theta_e, \mathscr{U}) p(\theta_e | \mathscr{U})}{\int p(\mathscr{D} | \theta_e, \mathscr{U}) p(\theta_e | \mathscr{U}) d\theta_e} \tag{7}$$

Where $p(\mathscr{D} | \theta_e, \mathscr{U})$ is the likelihood PDF, and $p(\theta_e | \mathscr{U})$ denotes a prior PDF for θ_e. In general, Gaussian probability distribution is chosen as a priori, which provides the largest prior uncertainty for θ_e, under the condition of barely information available. Therefore, the chosen Gaussian prior is stated as follows:

$$p(\theta_e | \mathscr{U}) = \mathscr{N}\left(0, \sigma_{\theta_e}^2 I\right) = \frac{1}{\left(2\pi\sigma_{\theta_e}^2\right)^{(n_p-1)/2}} \exp\left[-\frac{1}{2} \frac{\theta_e^{\mathrm{T}} \theta_e}{\sigma_{\theta_e}^2} \right] \tag{8}$$

in which $n_p = n_a + n_b + 1$ is assigned to be the dimension of uncertain parameter vector. What's more, $p(\mathscr{D} | \theta_e, \mathscr{U})$ is portrayed as follows for the likelihood function:

$$p(\mathscr{D} | \theta_e, \mathscr{U}) = \frac{1}{(2\pi\sigma^2)^{(n_d-n_s)/2}} \exp\left[-\frac{n_d - n_s}{2\sigma^2} J(\theta) \right] \cdot \frac{1}{(2\pi\sigma_0^2)^{n_s/2}} \exp\left[-\frac{1}{2\sigma_0^2} \sum_{j=1}^{n_s} y_j^2 \right] \tag{9}$$

in which n_d depicts the size of input and output data, and $y_j (j = 1, \cdots, n_s)$ are assumed to be independent and identically distributed (i.i.d.). with a variance σ_0^2 as the initial priori, that is, $y_j \sim \mathscr{N}(0, \sigma_0^2)$. $\boldsymbol{Y} = [y_{n_s+1} \cdots y_{n_d}]^{\mathrm{T}}, \boldsymbol{\Psi} = [\psi_{n_s+1}^{\mathrm{T}} \cdots \psi_{n_d}^{\mathrm{T}}]^{\mathrm{T}}, n_s = \max\{n_a, n_b + n_k - 1\}$, and $J(\theta) = \frac{1}{n_d - n_s} (\boldsymbol{Y} - \boldsymbol{\Psi}\theta)^{\mathrm{T}} (\boldsymbol{Y} - \boldsymbol{\Psi}\theta)$.

At the end, the posterior PDF equation (7) can be approximated by maximum likelihood estimate (MLE) as follows:

$$\widehat{\theta}_L = \arg\max_{\theta} p(\mathscr{D}|\theta_e, \mathscr{U}) = \arg\max_{\theta} J(\theta) = \left(\mathbf{\Psi}^{\mathrm{T}}\mathbf{\Psi}\right)^{-1}\mathbf{\Psi}^{\mathrm{T}}\boldsymbol{Y} \tag{10}$$

$$\widehat{\sigma}_L^2 = \arg\max_{\sigma^2} p(\mathscr{D}|\theta_e, \mathscr{U}) = \min J(\theta) = J(\widehat{\theta}_L) \tag{11}$$

$$C_{\theta}^{(L)} = \widehat{\sigma}_L^2\left(\mathbf{\Psi}^{\mathrm{T}}\mathbf{\Psi}\right)^{-1} \tag{12}$$

in which $\widehat{\theta}_L$ is the maximum likelihood estimates (MLE) of parameter vector θ, $\widehat{\sigma}_L^2$ is assigned as the maximum likelihood estimates of the variance with respect to prediction error, and $C_{\theta}^{(L)}$ is the covariance matrix of parameter $\widehat{\theta}_L$.Therefore, θ_e can be evaluated to determine the input/output model of the system for an ARX model class $\mathscr{U}(n_a, n_b, n_k)$.

The θ_e is reckoned with the requirement of a rational model order favored among model class $\mathscr{U}(n_a, n_b, n_k)$, which is pivotal to the successful execution of the ARX method. A reasonable order of ARX model is then singled out applying the classical Bayesian model selection. Propose a set of candidate model classes $\mathscr{M} = \cup\mathscr{U}$ for system, then, following Bayes' Theorem, the probability of $\mathscr{M}$ is stated as follows:

$$p(\mathscr{U}|\mathscr{D}, \mathscr{M}) = \frac{p(\mathscr{D}|\mathscr{U})p(\mathscr{U}|\mathscr{M})}{p(\mathscr{D}|\mathscr{M})} \tag{13}$$

In which $p(\mathscr{D}|\mathscr{U}) = \int p(\mathscr{D}|\theta_e, \mathscr{U})p(\theta_e|\mathscr{U})d\theta_e$ is generally pronounced as the *evidence* for a model class $\mathscr{U}$ beneath the condition of available data. Due to the reason that prior probability $p(\mathscr{U}|\mathscr{M})$ for each model class $\mathscr{U}$ is quite often assumed to be uniform, the posterior probability $p(\mathscr{U}|\mathscr{D}, \mathscr{M})$ of each model class $\mathscr{U}$ is therefore determined by the evidence. Suppose $\mathscr{U}$ is globally identifiable given data $\mathscr{D}$ and the number of data, n_d, is sufficiently large, then the evidence can be well estimated by Laplace asymptotic approximation, the logarithm of the estimated evidence finally equal as follows [32]:

$$\begin{aligned}\ln p(\mathscr{D}|\mathscr{U}) = &-\frac{n_d - n_s}{2}\ln(2\pi) - \frac{n_d - n_s - n_p + 1}{2}\ln\left(\widehat{\sigma}_L^2\right) - \frac{n_d - n_s}{2} - \left(n_p - 1\right)\ln\theta^* - \frac{1}{2}\frac{\widehat{\theta}_L^T\widehat{\theta}_L}{\theta^{*2}} \\ &-\frac{1}{2}\ln\left(\frac{n_d - n_s}{2}\right) - \frac{1}{2}\ln\det\left[\mathbf{\Psi}^{\mathrm{T}}\mathbf{\Psi}\right] - \frac{n_s}{2}\ln\left(2\pi\sigma_0^2\right) - \frac{1}{2\sigma_0^2}\sum_{j=1}^{n_s} y_j^2\end{aligned} \tag{14}$$

in which θ^* equals to the utmost element among the maximum likelihood estimates $\widehat{\theta}_L$, by which the estimates, $\widehat{\theta}_L$ will be in the relatively high probability region of priors.

After all, the values of evidence can be calculated analytically through equation (14), thus, the posterior probability of ARX models with different model orders can also be determined from equation (13). Then, the model order is selected whose posterior probability of ARX model is the maximum a posteriori (MAP) value.

3.1.2. Parameter estimates of ARX model

In the ARX model, the natural frequencies f_j and damping ratios ξ_j denote the modal parameters of the j th mode, which are able to be connected to the model coefficients $\theta = [a_1 \cdots a_{n_a}\ b_1 \cdots b_{n_b}]^{\mathrm{T}}$, while model coefficients of ARX model are estimated by maximum a posteriori estimation or maximum likelihood estimation, once model order is selected from above equations 7–14. The natural modes are then reckoned as follows [48–50]:

$$f_j = \frac{\left|\log p_j\right|}{2\pi\Delta t} = \frac{\ln\left(1/r_j\right)}{2\pi\xi_j\Delta t} \tag{15}$$

$$\xi_j = \frac{-\left|\log p_j\right|}{2\pi f_j\Delta t} = \frac{\ln\left(1/r_j\right)}{\sqrt{\left(p_j\right)^2 + \left[\ln\left(1/r_j\right)\right]^2}} \tag{16}$$

In which p_j and $\overline{p}_j$ are assigned as the j th conjugate pair of the poles of the polynomial functions, which is the roots of denominator $A(z) = 0$. r_j and $\overline{r}_j$ are also the j th conjugate pair of the corresponding residues of the system, which can be derived from the partial fractions expansion of the transfer function between the input to the output:

$$TransferFunction = \frac{B(z)}{A(z)} = Consant + \sum_{j=1}^{n_a/2}\left[\frac{r_j}{1 - p_j z^{-1}} + \frac{\overline{r}_j}{1 - \overline{p}_j z^{-1}}\right] \tag{17}$$

3.2. Identification results using actual monitoring data

In this study, ARX model method with model order determined by Bayesian model selection method introduced in the previous sections, is carried out using records obtained through structural health monitoring system of a passively controlled eight-story steel building. To testify the effectiveness of the Bayesian based order selection of auto-regressive exogenous (ARX) model method developed in the previous section, an earthquake record used for analysis here as an example is a recorded data set of a large earthquake with a moment magnitude of 7.0 on 26$^{\text{th}}$ May 2003. Among all four strong earthquake recordings, the records on 26$^{\text{th}}$ May 2003 were set on from perfect initial condition with all devices on explicit preset position, since it's the first strong event occurred on

the building. Besides, both the building and monitoring devices are functional well without any damage before, during, and after the strike of strong earthquake on 26th May 2003. These earthquake records occurred in Sendai located in the Miyagi Prefecture of Japan, and elaborate information about the time and location, depth of these earthquakes, epicentral distance as well as magnitude are listed in Table 1.

In order to implementation of ARX model, the acceleration time history on the ground of 1st story is designated to be the input excitation and the recorded data of other stories are appointed as the outputs. Then, the factor of soil–structure interaction could be considered to be ignorable, since the ground acceleration of the 1st story is reckoned as the input instead the free-field ground acceleration records. Besides, the effect of torsional motion is very small due to the symmetrical plan of the structure, thus, the natural modes are estimated for both horizontal directions (that is, horizontal and transverse directions, respectively). Here, the horizontal accelerations denote the north–south (NS) orientation and east–west (EW) direction with respect to longitudinal and transverse directions of the building (named after 'EW' and 'NS' hereinafter).

A segment of time from 15 s to 60 s which includes the maximum response in each direction is selected to extract dynamic properties of the passively-controlled eight-story steel building, since the first 15s is basically the start-up part and full of noise. Fig. 2 displays the recorded acceleration response time histories of the building in both directions. The recorded signals are processed through a 20th-order lowpass Butterworth filter with a cut-off frequency of 20 Hz, which is much more than the natural frequencies of interest, which are generally in the lower-frequency region up to 6 Hz. The sampling interval is 0.005 s.

Bayesian model selection is conducted to determine an appropriate model order based on various model class $\mathscr{U}(n_a, n_b, n_k)$, for which the range of model orders n_a, n_b and n_k have following restraint conditions: (1) n_k is assigned to be the time delay, as the time delay is quite small for most case, therefore generality was set to 0; (2) n_a is order of output of the system, which usually was set to be an even figure, as practical systems generally present plural mode form in which one structural mode is in conformity with a pair of conjugate poles of the system, that is, $n_a = 2p$; (3) n_b has ensuing interrelationship with n_a, i.e. $n_b = n_a + 1$, which can be corroborated by the contrast of partial fraction expansions of the transfer function between continuous time in the Laplace plane and discrete time in the Z plane. Accordingly, $n_s = \max\{n_a, n_b + n_k - 1\} = n_a$,and the dimension of parameters $n_p = n_a + n_b + 1 = 2n_a + 2$. In order to adequately cover the appropriate orders of model that need to be determined, the range of chosen candidate model classes are as follow:

$$\{\mathscr{U}_d = \mathscr{U}(n_a, n_a + 1, 0) : n_a = 4, 6, \ldots, 22, 24\} \tag{18}$$

The posterior probability of ARX patterns with varied orders are then calculated using Bayes' Theorem equation (14), and is shown as follows in Table 2. From Table 2, the ARX model with $n_a = 16$ holds the uppermost posterior probability for both directions.

Though the order of model has been resolved, segregating the 'true' modes from 'false' ones can still be a huge challenge as before. As the selected model orders are generally far bigger than twice the number of significant modes, which contribute most of the structural response, thus, the 'false' numerical modes are provoked into the identified modes, which stemmed from the estimation of the coefficients of ARX model. To consistently single out the 'true' modes that are about to be utilized for the next section, stabilization chart is employed to discern actual modes from false ones. The stabilization chart is capable of reflecting the relative differences of each

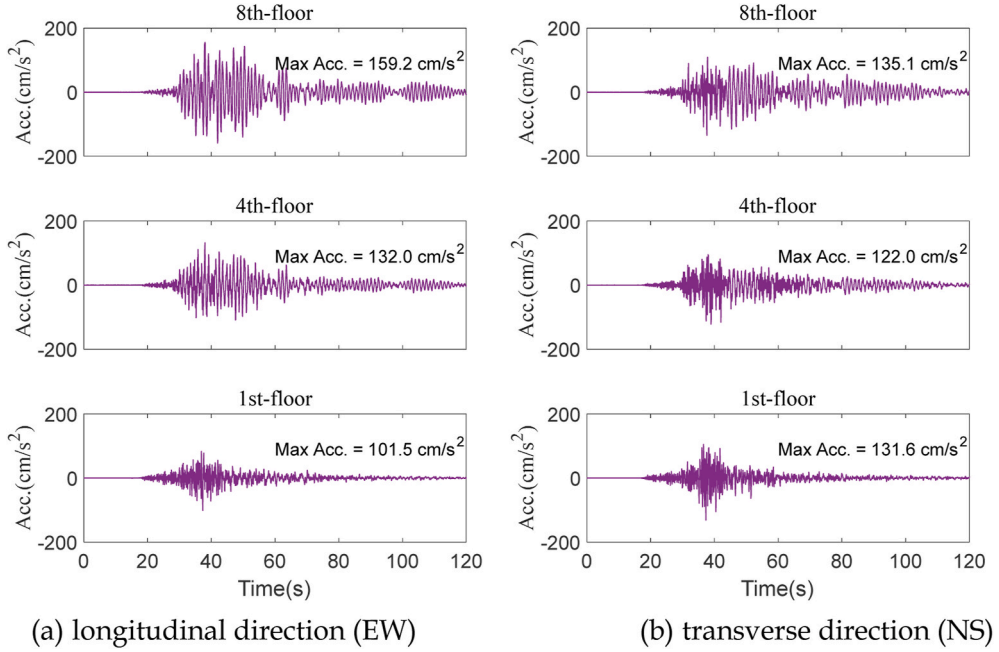

Fig. 2. Acceleration time histories of input and output: (a) longitudinal direction (EW) (b) transverse direction (NS).

Table 2
Posterior probability of ARX models for varied orders.

n_a	…	6	8	10	12	14	16	18	20	…
$P(\Upsilon)(\%)$(EW)	…	0.0	0.0	0.0	0.0	0.0	88.9	11.1	0.0	…
$P(\Upsilon)(\%)$(NS)	…	0.0	0.0	0.0	0.0	0.0	92.7	7.3	0.0	…

modes which are estimated under two adjacent orders. Therefore, real modes can distinguish themselves from the spurious modes by comparing the dynamic properties of these two groups. In practice, the relative differences are defined as less than 1% for the natural frequencies, 5% for damping ratios and 10% for modal assurance criterion (MAC) index of mode shapes, which are used to check the consistency of the modal properties derived from two approaches. In addition, modal phase collinearity (MPC) index is also employed to try to obtain stable modes [51]. The modal phase collinearity (MPC) index is very much close to 1 for an actual structural mode, and so the MPC index is set to be no less than 0.9 in this study. Afterall, the stabilization diagram figured out for ARX model is exhibited in Fig. 3. What's more, Fig. 3 also depicts the estimated transfer function curve for comparing.

As can be seen from Fig. 3 that first three significant modes are identified, which contribute most of the structural response. The identified first three significant modes of the building are listed as follows in Table 3. The same processes are conducted to the other three strong earthquake recordings, the identified first three natural frequency and damping ratio are also shown in Table 3. From the observation of identified results, the first two natural frequency for records 2003/5/26, 2005/8/16 and 2011/3/9 are basically the same level, so are the first two damping ratio. Nevertheless, Great East Japan earthquake struck northeastern Japan on March 11, 2011, the steel building experienced the earthquake with all oil dampers on the first floor completely destroyed with abutment breakage, besides, dampers on the third and fourth floors had severe oil leakages. Right after the 3•11 earthquake, another strong earthquake was recorded on April 7th, 2011, which provided an opportunity to investigate the actual dynamic properties of main steel frame of the building. Post-earthquake inspection showed that the main steel frame was intact without damage. However, the identified first two fundamental frequency and damping ratio decrease significantly for records 2011/4/7, as can be observed in Table 3. Two main aspects may account for this phenomenon, on one hand, the connections and non-structural elements may undergo some micro damage which can't be inspected by visual. On the other hand, the decrease of both frequency and damping ratio indicates that the oil damper braces not only provide supplemental damping, but also offer additional stiffness to the steel building.

In practice, it's most often the common case that sensors are only available on selected floors due to cost. In this paper, the number of monitoring instruments arranged on the steel building studied is also limited. As described in section 2.2, only the horizontal directions (including the long side direction and the short side direction) of the 1st, 4th and 8th floors are deployed with accelerometers, respectively. Therefore, the degree of freedom of the actual measurement of the structure is only 1 layer, 4 layers and 8 layers. Since the degrees of freedom monitored will determine the integrity of the identifiable mode shapes of the structural system, that is, the corresponding mode shapes of the floors with monitoring records can be identified, otherwise, the mode shapes at the corresponding floors are unknown. Mode shape expansion techniques were then employed to approximate the unmeasured mode shape vectors. Finally, the expanded first three intact mode shapes of the steel building are illustrated in Fig. 4, and are about to be used for further analysis in next section.

4. Additional damping ratio for the nonlinear oil damper

In this paper, the different damping states also provide a good opportunity to probe the damping characteristics of passively-controlled steel building. This section presents simplified estimations aiming to quantify the additional damping ratios offered by added dampers. Before that, the oil dampers installed on every floor of the passively-controlled steel building are introduced, what's

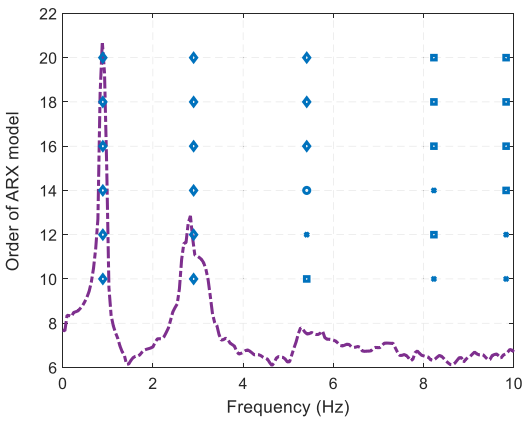

Fig. 3. Stabilization diagram for autoregressive with exogenous term (ARX) model (symbol diamond denotes stable mode, square denotes stable frequency & mode shape, circle denotes stable frequency & damping, cross denotes stable frequency, dotted line denotes frequency response function).

Table 3
Estimates of modal parameters (EW).

Records	f_1/Hz	f_2/Hz	f_3/Hz	ξ_1	ξ_2	ξ_3
2003/5/26	0.892	2.885	5.399	0.031	0.051	0.061
2005/8/16	0.86	2.803	5.262	0.03	0.05	0.065
2011/03/09	0.852	2.761	5.4	0.028	0.046	0.069
2011/04/07	0.759	2.4	5.61	0.018	0.037	0.076

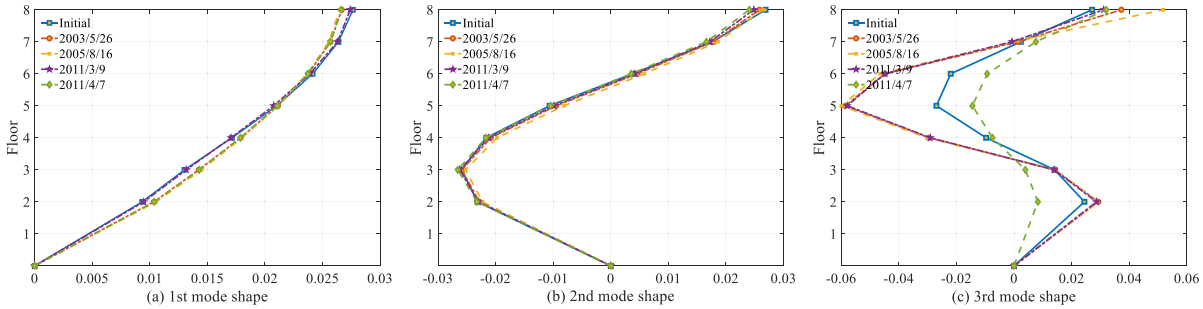

Fig. 4. Mode shapes of the building (EW).

more, analytical model determination and parameters identification of nonlinear oil damper are conducted sequentially. Following that, the additional equivalent damping ratios supplied by the nonlinear oil damper braces are reckoned through the determined analytical models. In the end, the supplemental damping ratios provided by all the added dampers are deducted and evaluated by employing the identified damper parameters and the modes information derived from the system identification in above section.

4.1. Analytical model for oil damper

The oil dampers mounted on the steel building consist of a cylinder and a pair of pistons and are connected through the V-type steel braces between the adjacent floors. The interstices between the cylinder and pistons are stuffed by viscoelastic polymer to allow for easy production, the pair of pistons are installed in the U-type abutment which is fixed on the floor, while the central cylinder is mounted onto the V-type brace. The dimension of the nonlinear oil damper is 424 mm wide and 328 mm high, moreover, two types of nonlinear oil dampers with different orifice specifications and stroke limits of relief mechanism are utilized for 1st floor (Type I) and 3rd to 8th floor (Type II), respectively. Detail construction of the nonlinear oil dampers are as illustrated in Fig. 5 and 6.

The viscoelastic material shapes soft rings functioning to seal pressurized liquid, additionally, produces viscoelastic resisting force when the dynamic shear deformation enforces on sealing rings. Another primal member of resisting force supplied by the nonlinear oil damper stems from inner pressure differential of liquid when oil flows through the narrow orifice. Experimental tests have also been carried out to probe the behavior and hysteresis characteristic of both the viscoelastic soft rings and inner viscous liquid flowing through the orifice, respectively. According to the observations, hysteresis curves of the viscoelastic resisting force in the condition of the damper with hollow cavity create a shape of ellipse bearing an obvious axial tendency, which has a positive correlation with the excitation frequency. Though the simple Maxwell model is capable of simulating the elliptical loops, nevertheless, it discloses a significant frequency dependence, which indicates a much larger bevel angle of the axis for a small increased frequency [52]. What's more, hysteresis curves for the Maxwell model generally have a phenomenon of phase-lag for displacement at zero [53]. Overall, the dynamic behaviors and hysteresis loops of the nonlinear oil damper are much closer to that of a Kelvin-Voigt model. Therefore, a

Fig. 5. Intact oil damper.

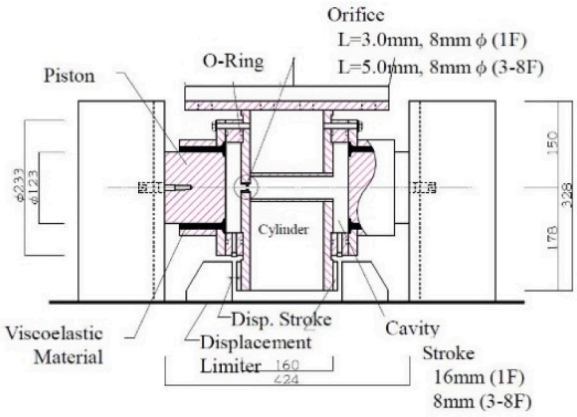

Fig. 6. Schematic diagram of the nonlinear oil damper.

Kelvin-Voigt model is exploited to modeling the dynamic behaviors of the nonlinear oil damper, additionally, the accuracy of the Kelvin-Voigt model is also examined.

The generalized Kelvin-Voigt model comprises of a spring and a nonlinear dashpot in parallel. Additionally, through the parallel combination, the model can allow for both the velocity-dependent and displacement-dependent elastic restoring force at the same time. Fig. 7 depicts the schematic diagram of the generalized Kelvin-Voigt model. Further, the mathematic expression of dynamic equilibrium equation for the oil damper brace can be written as follows:

$$F_d(t) = k_d x_d(t) + sign(\dot{x}_d(t)) c_d |\dot{x}_d(t)|^{\alpha_d} \tag{19}$$

Where $F_d(t)$ and $x_d(t)$ are the axial force and displacement of oil damper brace, respectively, k_d is the stiffness coefficient, c_d is the viscous damping coefficient, α_d is the velocity exponent and sign(·) is assigned as the signum function, The exponent coefficient α_d renders an expression on the nonlinearity of the constitutive behavior and characterizes the design of orifice and viscous material used. For $\alpha_d = 1$, the damper force is linearly varied with the velocity. While for $\alpha_d = 0$, the hysteresis curves between damper force and displacement are rectangular, which is typical representation for friction damper [54]. For $\alpha_d > 1$, the nonlinear damper may generate large forces under high velocity demands, which produces large interaction force transferring to the connections and structure of the building, however, this phenomenon is absolute undesirable in seismic design applications. Therefore, $\alpha_d \leq 1$ is mostly adopted for practical seismic applications. At the same time, a relief mechanism is usually introduced to restrict the maximum damper force enforced in extreme case, e.g. intense ground motion strikes. Thus, the maximum damper force of the oil dampers could be kept within a reasonable range.

Structure health monitoring devices were also deployed on the nonlinear oil dampers, a load cell device was carried out on the tail of the nonlinear oil damper brace for the purpose of gauging the damper force. Displacement sensors were set up to gauge the axial relative displacement of the nonlinear oil damper in the track direction. Take an assumption that the stiffness of the rigid V-type braces is infinite and the corresponding deformation is negligible, consequently, the displacement of oil damper brace equals to the inter-story drift. Detailed distribution about the position of sensors were displayed in Fig. 8. Fig. 9 plots the recorded data of damper force verse displacement for damper brace on May 26th, 2003.

4.2. Oil damper identification by particle Markov chain Monte Carlo

The mathematical model for the nonlinear oil damper brace is crucial to be incorporated into structural computational models, and for successful application in design practice, as well as for model updating and prediction using vibration data in structural health monitoring. With the progress of the nonlinear oil dampers from theoretical designs into practical applications, reliable methods for

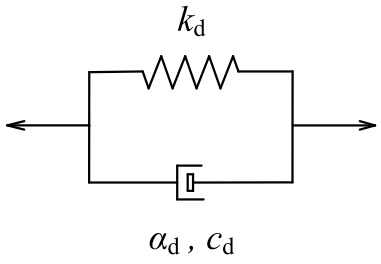

Fig. 7. Schematic diagram of Kelvin-Voigt model.

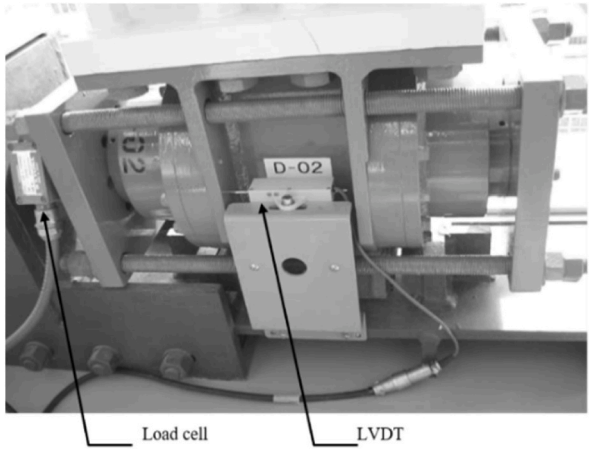

Fig. 8. Detailed position distribution of sensors.

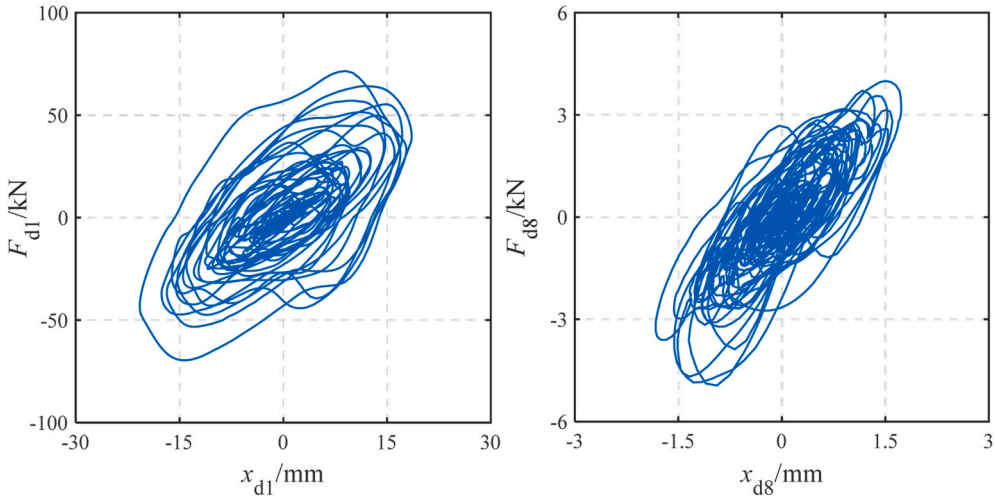

Fig. 9. Force–deformation hysteresis loops.

nonlinear model identification are necessary to assess if the damper is working as designed and validate the expected performance in the steel building. To further explore the damping properties and hysteresis behaviors of the nonlinear oil dampers with viscoelastic polymer packing soft rings under earthquake excitations, Particle filter improved with Metropolis-Hastings algorithm is exploited to estimate the model parameters of the nonlinear oil damper, which can be represented mathematically by a nonlinear Kelvin-Voigt model.

4.2.1. Particle Markov chain Monte Carlo methodology

Consider the class of nonlinear dynamical systems modeled by the probabilistic model described in Fig. 10, in which x_k denotes the

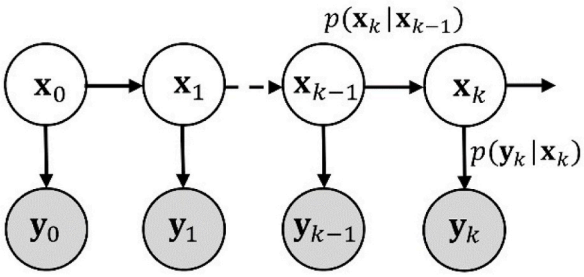

Fig. 10. Probabilistic model of generalized dynamical system.

unobserved states of the nonlinear dynamical system (or hidden variables) at time instant $t = k\Delta t$, and y_k is assigned to be the observations of the system measured at time instant $t = k\Delta t$. While $p(x_k|x_{k-1})$ expresses the state evolution function of the system, which is also referred to be as the Markovian transmission density. Besides, $p(y_k|x_k)$ signifies the emission density of the system. General problem encountered by the class of nonlinear dynamical systems is that estimation of the latent variables is demanded provided by the entire set of measurements $y_{1:k}$. Henceforth, for any generic sequence $y_{1:k}$ implies $(y_1, y_2, \cdots, y_k)$. This general difficulty can be tackled from a Bayesian perspective view through shifting the problem into determining an estimation of the conditional posterior $p(x_k|y_{1:k})$. Following Bayes' law, posterior distribution $p(x_k|y_{1:k})$ can be written as:

$$p(x_k|y_{1:k}) = \frac{p(y_k|x_k)p(x_k|y_{1:k-1})}{p(y_k|y_{1:k-1})} \tag{20}$$

However, the analytical solution for posterior density $p(x_k|y_{1:k})$ does not exist except for particular cases, hence, numerical approximation algorithms are developed to evaluate the density-weighted integrals from above equation. Among these stochastic simulation methods, Monte Carlo estimation methods provide a numerical way of calculating the density-weighted integrals using a set of samples instead of closed form computation of statistical quantities. Thus, the perplexed integrations are turned into the summation of the weighted samples that are distributed according to the desired target density. The accuracy, efficiency and convergence of the Monte Carlo methods have been verified by the central limit theorem [55]. Additionally, the error can be expressed as $O(N^{-1/2})$, where N is assigned as the dimension of samples. Since the error item has nothing to do with the dimensionality of the hidden variables x, Monte Carlo approximation methods have the superior advantage over practically other numerical algorithm for the case with large amount of latent variables in theory [56,57]. Nevertheless, it is not necessary in practice [58,59]. Besides, Monte Carlo approximation is capable of applying to nonlinear systems and non-Gaussian densities.

In practice, it's not very often able to sample directly from posterior density $p(x_k|y_{1:k})$ due to the complicated functional form, which is especially the case for the target density of following properties: multivariate and non-Gaussian or even unknown [60]. While importance sampling provides a way to sample from importance density instead, where an approximate distribution is proposed as an importance distribution to draw samples from Ref. [55]. In this paper, sequential importance sampling (SIS) particle filters (PF) are implemented to estimate the posterior distribution of states and parameters of the oil damper based on the noisy measurements of the system.

Consider the generic state space model of a dynamic system as follows:

$$x_k = g(x_{k-1}, w_k) \tag{21}$$

$$y_k = h(x_k, v_k) \tag{22}$$

where $g(\cdot)$ is assigned as the state transition function and $h(\cdot)$ represents the observation function. $w_k \sim N(0, Q_k)$ represents the process noise vector, which describes the model error including those parts of true transition function that are not modeled, noise in measured inputs and/or unmeasured inputs. $v_k \sim N(0, \mathrm{R}_k)$ is the measurement noise, used to model noise in measured observations. Moreover, noise is supposed to be additive, and be propagated through transition function and measurement equation.

Determining the estimation of the conditional posterior $p(x_k|y_{1:k})$ is desired, in order to realize that, first an importance density $q(x_k|y_{1:k})$ was chosen with the same support and its maximum in roughly the same place as $p(x_k|y_{1:k})$. Then, a weighting factor was defined and deducted by

$$W(x_k) \triangleq \frac{p(x_k|y_{1:k})}{q(x_k|y_{1:k})} = \frac{p(y_k|x_k)p(x_k|y_{1:k-1})}{p(y_k|y_{1:k-1})} \frac{1}{q(x_k|y_{1:k})} \tag{23}$$

Since $p(y_k|y_{1:k-1})$ is just a Bayesian normalization constant, the weight function $W(x_k)$ can be rewritten as

$$W(x_k) \propto \frac{p(y_k|x_k)p(x_k|y_{1:k-1})}{q(x_k|y_{1:k})} \tag{24}$$

In which $\propto$ represents a proportionality. the weight function $W(x_k)$ can then be evaluated recursively by way of solving the Chapman–Kolmogorov equation. Thus, above equation (24) becomes

$$W(x_k) \propto \frac{p(y_k|x_k)\int p(x_k|x_{k-1}, y_{1:k-1})p(x_{k-1}|y_{1:k-1})dx_{k-1}}{\int q(x_k|x_{k-1}, y_{1:k})q(x_{k-1}|y_{1:k-1})dx_{k-1}} = \frac{p(y_k|x_k)\int p(x_k|x_{k-1})p(x_{k-1}|y_{1:k-1})dx_{k-1}}{\int q(x_k|x_{k-1}, y_{1:k})q(x_{k-1}|y_{1:k-1})dx_{k-1}} \tag{25}$$

Here, $p(x_k|x_{k-1}, y_{1:k-1}) = p(x_k|x_{k-1})$ is under the assumption that state evolution equation is a first-order Markov process independent of the observations.

Then, a set of random samples $\{x_{k-1}^{(i)}, i = 1, \ldots, N_s\}$ are sampled from the importance density $q(x_{k-1}|y_{1:k-1})$, that is, $x_{k-1}^{(i)} \sim q(x_{k-1}|y_{1:k-1})$. N_s is the number of particles. Propagating these samples through above equation (25) gets

$$\widetilde{W}_k^{(i)} = \sum_{i=1}^{N_s} \frac{p(y_k|x_k)p\left(x_k\middle|x_{k-1}^{(i)}\right)p\left(x_{k-1}^{(i)}\middle|y_{1:k-1}\right)}{q\left(x_k\middle|x_{k-1}^{(i)}, y_{1:k}\right)q\left(x_{k-1}^{(i)}\middle|y_{1:k-1}\right)} = \sum_{i=1}^{N_s} \widetilde{W}_{k-1}^{(i)} \frac{p(y_k|x_k)p\left(x_k\middle|x_{k-1}^{(i)}\right)}{q\left(x_k\middle|x_{k-1}^{(i)}, y_{1:k}\right)} \tag{26}$$

Generating samples $\{x_k^{(i)}, i=1,\ldots,N\}$ at time step k from $q(x_k|x_{k-1}^{(i)},y_{1:k})$, that is, $x_k^{(i)} \sim q(x_k|x_{k-1}^{(i)},y_{1:k})$ and approximating $q(x_k|y_{1:k})$ using the set of Dirac delta function by $q(x_k|y_{1:k}) = \frac{1}{N_s}\sum_{i=1}^{N}\delta(x_k - x_k^{(i)})$.Thus, posterior distribution density can be expressed as

$$p(x_k|y_{1:k}) = \sum_{i=1}^{N_s} \widetilde{W}_{k-1}^{(i)} \frac{p\left(x_k\middle|x_{k-1}^{(i)}\right)}{q\left(x_k\middle|x_{k-1}^{(i)},y_{1:k}\right)} p(y_k|x_k)q(x_k|y_{1:k}) = \sum_{i=1}^{N_s} \frac{\widetilde{W}_{k-1}^{(i)}}{N_s} \frac{p\left(x_k^{(i)}\middle|x_{k-1}^{(i)}\right)}{q\left(x_k^{(i)}\middle|x_{k-1}^{(i)},y_{1:k}\right)} p\left(y_k\middle|x_k^{(i)}\right)\delta\left(x_k - x_k^{(i)}\right) \tag{27}$$

Normalizing $\frac{\widetilde{W}_{k-1}^{(i)}}{N_s}$ by $W_{k-1}^{(i)} = \frac{\widetilde{W}_{k-1}^{(i)}/N_s}{\sum_{i=1}^{N}\widetilde{W}_{k-1}^{(i)}/N_s}$, so that they sum up to unity.

Ultimately, the recursive weight update equation is derived as

$$W_k^{(i)} = W_{k-1}^{(i)} \frac{p\left(x_k^{(i)}\middle|x_{k-1}^{(i)}\right)}{q\left(x_k^{(i)}\middle|x_{k-1}^{(i)},y_{1:k}\right)} p\left(y_k\middle|x_k^{(i)}\right) \tag{28}$$

where $p(x_k^{(i)}|x_{k-1}^{(i)})$ is the predictive density (or transitional density) defined by the process equation (22) and $p(y_k|x_k^{(i)})$ is the likelihood function expressed by the measurement equation (22). The selection of the importance density $q(x_k^{(i)}|x_{k-1}^{(i)},y_{1:k})$ is crucial to the PF implementation, researches have validated that the optimal importance density is the one that minimizes the variance of the true weights, which is written as follows :

$$q\left(x_k\middle|x_{k-1}^{(i)},y_{1:k}\right)_{opt} = q\left(x_k\middle|x_{k-1}^{(i)},y_k\right) = \frac{p\left(x_k\middle|x_{k-1}^{(i)}\right)p\left(y_k\middle|x_k,x_{k-1}^{(i)}\right)}{p\left(y_k\middle|x_{k-1}^{(i)}\right)} \tag{29}$$

the Equation $q(x_k|x_{k-1}^{(i)},y_{1:k})_{opt} = q(x_k|x_{k-1}^{(i)},y_k)$ signifies that the selected importance density at current time step k depends on only x_{k-1} and y_k at previous time step. However, taking samples from $q(x_k|x_{k-1}^{(i)},y_k)$ might still not be direct, giving rise to suboptimal choice of the transitional prior as the importance density function

$$q\left(x_k\middle|x_{k-1}^{(i)},y_{1:k}\right) = p\left(x_k\middle|x_{k-1}^{(i)}\right) \tag{30}$$

By substituting above equation (30) into equation (28), the recursive weight update equation is reduced to

$$W_k^{(i)} = W_{k-1}^{(i)} p\left(y_k\middle|x_k^{(i)}\right) \tag{31}$$

Thus, the estimated posterior density distribution at time step k equals

$$\widehat{p}(x_k|y_{1:k}) = \sum_{i=1}^{N_s} W_k^{(i)}\delta\left(x_k - x_k^{(i)}\right) \tag{32}$$

In addition, an estimation of marginal likelihood $p(y_{1:k})$ can also be obtained through the above particle filter algorithm by

$$\widehat{p}(y_{1:k}) \triangleq \widehat{p}(y_1)\prod_{n=2}^{k}\widehat{p}(y_k|y_{1:k-1}) \tag{33}$$

In which

$$\widehat{p}(y_k|y_{k-1}) = \frac{1}{N_s}\sum_{i=1}^{N_s} W_k\left(x_k^{(i)}\right) \tag{34}$$

Overall, samples $\{x_k^{(i)}, i=1,\ldots,N\}$ at time step k drawn from $q(x_k|x_{k-1}^{(i)},y_{1:k})$ is actually generated by the transitional density, namely, $x_k^{(i)} \sim p(x_k|x_{k-1}^{(i)})$.Besides, the recursive updated weight is up to the likelihood function, the likelihood mostly used is a Gaussian distribution to gauge the difference between the estimates and the corresponding measurements. Alternatively, empirical likelihoods or numerical likelihoods can also be used [61,62].

Particle filters are able to obtain the whole posterior density distribution rather than allow for only estimations of first two moments, whereas a significant practical problem with particle filter is the degeneracy of the particles, which refers to that the weights of all except for a few are almost zero as a result of several iterations. The degeneracy can be mitigated through a resampling process. However, another problem of losing diversity among the particles emerges due to the resampling, as the resampled particles will have many duplicated particles with given high weight, which becomes severe under small process noise case [63,64].

Among these methods to rectify the sample impoverishment [36,56,65–67], Metropolis-Hastings sampling algorithm is capable of applying to large tail probabilities. Although computationally intensive, Markov Chain Monte Carlo (MCMC) method builds efficient

proposal distribution to generate ergodic chain whose stationary distribution follows the target PDF. In this research, posterior density $p(x_{1:k}|y_{1:k})$ is the target PDF as in equation (28). It is usually impossible to sample directly from $p(x_{1:k}|y_{1:k})$, MCMC algorithm builds proposal distribution to produce samples efficiently, which asymptotically follows the distribution of the target PDF when the number of Markov steps increases.

Particle filter improved with Metropolis-Hastings (PFMH) algorithm [34–36] engages the estimates from particle filter, $\hat{p}(x_{1:k}|y_{1:k})$, as a proposal distribution, which is not necessary to be accurate or trusty, but just roughly endures the target distribution, $p(x_{1:k}|y_{1:k})$. Nevertheless, the marginal density of particles doesn't have analytical expression, which is necessary for calculating the crucial MH acceptance ratio. In order to tackle this difficulty, a marginal likelihood $p(y_{1:k})$ is adopted as sampler, whose support includes all random variables generated by above particle filter method. Overall, a PFMH algorithm is depicted as follows:

Initialization: $i=1$

(a) Determine the number of iterations N and proposal distribution $q=\hat{p}(x_{1:T}\,|\,y_{1:T})$ for MCMC samplers

(b) Select the initial state prior distribution of the latent Markov process $\pi(x_1)$ as important density, i.e. take $q(x_1\,|\,y_1)=\pi(x_1)$, reckon the desired density $X_{1:T}^{(1)}=\hat{p}^{(1)}(x_{1:T}\,|\,y_{1:T})$ and homologous marginal likelihood $\hat{p}^{(1)}(y_{1:k})$ by particle filter using equations. (24)-(35).

Iteration: while $i=2:N$

(a) Propose a move to state variables using the proposal distribution $q=\hat{p}^{(i-1)}(x_{1:T}\,|\,y_{1:T})$

(b) Run particle filter with the proposed state as initial state prior distribution, obtain particles $X_{1:T}^{*}\sim\hat{p}^{(i)}(x_{1:T}\,|\,y_{1:T})$ and corresponding marginal likelihood $\hat{p}^{*}(y_{1:k})$.

(c) Calculate the acceptance ratio

$$\log(\alpha^{i})=\min\left\{\log(1),\log\left(\frac{\hat{p}^{*}(y_{1:k})}{\hat{p}^{(i-1)}(y_{1:k})}\right)\right\}$$

(d) Generate a variate $u\sim uniform[0,1]$

(e) If $\log(u)<\log(\alpha^{i})$, accept the move and set $X_{1:T}^{(i)}=X_{1:T}^{*}$, and $\hat{p}^{(i)}(y_{1:k})=\hat{p}^{*}(y_{1:k})$; otherwise set $X_{1:T}^{(i)}=X_{1:T}^{(i-1)}$, and $\hat{p}^{(i)}(y_{1:k})=\hat{p}^{(i-1)}(y_{1:k})$

T is assigned as the length of measurement, y. Since the initial state x_1 follows the prior distribution rather than the target posterior, it consumes some time for the special designed Markov Chain to dive into high probability region of desired density, which usually be referred to "burn-in". Therefore, in order to obtain a well-established Markov Chain [68], the acceptance ratio should be within range [0.15 0.4]. Furthermore, the objective of PFMH algorithm is to approximate the posterior $p(x_{1:T}|y_{1:T})$, by the way, also yields an approximation to its normalizing constant $p(y_{1:T})$, which can be applied for Bayesian model updating, model class selection, and model averaging. In practice, parameters are generally the desired target, which can be estimated through an augmented state vector with parameters.

4.2.2. Implementation

The PFMH algorithm is carried out to the nonlinear oil dampers with states and parameters identification simultaneously through an augmented state vector with parameters approach. Prior information about dynamic characteristics of the oil damper can be leveraged to be at similar orders of magnitude allowing for visiting parameter space evenly for every parameter, thus enhance the model for PFMH implementation [69]. In this study, the scale of theoretical value for every parameter is utilized to establish the augmented state vector for parameters and state joint identification with PFMH. What's more, the log transformation can guarantee parameters constrained to positive domain and the states value could be negative or positive. which achieves a nearly unconstrained optimization on the parameters. Thus, no additional instabilities could be induced into the identification process.

$$X=\left[x,\dot{x},\log\left(\frac{c_{\mathrm{d}}}{100}\right),\log\left(\frac{k_{\mathrm{d}}}{1000}\right),\log\left(\frac{\alpha}{1}\right)\right]^{\mathrm{T}}=[x_1,x_2,x_3,x_4,x_5]^{\mathrm{T}} \tag{35}$$

The discrete state transition equation can be expressed as

$$g\left(x_k,\ddot{x}_g\right)=x_{k-1}+\int_{(k-1)\Delta t}^{k\Delta t}g\left(x_{k-1},\ddot{x}_g\right)+w_k \tag{36}$$

$$g\left(x_{k-1},\ddot{x}_g\right)=\begin{bmatrix}\dot{x}_1\\ \dot{x}_2\\ \dot{x}_3\\ \dot{x}_4\\ \dot{x}_5\end{bmatrix}=\begin{bmatrix}x_2\\ (sign(x_2)(F_{\mathrm{d}}(t)-k_{\mathrm{d}}x_1)/c_d)^{1/\alpha_{\mathrm{d}}}\\ 0\\ 0\\ 0\end{bmatrix} \tag{37}$$

In a similar way, the discrete observation equation is expressed as

$$h\left(x_k,\ddot{x}_g\right)=\begin{bmatrix}x_1\\ (sign(x_2)(F_d(t)-k_dx_1)/c_d)^{1/\alpha_d}\end{bmatrix}+v_k \tag{38}$$

The relative displacement x and the absolute acceleration $\ddot{x}+\ddot{x}_g$, of the oil damper are the measurement vectors, which x is

observed from the LVDT as Fig. 8. As we can tell, one end of LVDT is set on the oil damper, and the other end is mounted on the floor, thus, the relative axial displacement of the oil damper in the track direction could be measured. $\ddot{x}_g$ is the records by the accelerometer set up on the corresponding floor.

Assumption is made that the process noise of the system is incurred primarily due to noise in the input. thereupon, process noise covariance matrix (Q) is a 5 × 5 diagonal matrix, in which only q_{11} and q_{22} is non-zero. Likewise, the measurement noise covariance matrix (R) is a 2 × 2 diagonal matrix with non-zero entry r_{11} and r_{22}, which are the variances of the corresponding measurement noise in the displacement and acceleration responses of the nonlinear oil damper, respectively. Moreover, it's assumed that the measurement noises in the various sensors are independent with each other. Then, the prior distribution for each parameter is chose as follows at initial step: c_d and k_d are assigned to be normal distribution, parameter α is appointed to be uniform distribution, covariance for the corresponding process noise q_{11}, q_{22}, and measurement noise r_{11}, r_{22} are assigned as inverse gamma distribution. Gaussian likelihood is exploited to gauge the difference between the estimates and the measurements. Thus, the likelihood can be conveyed as follows:

$$p(y_k|x_k) = \frac{1}{\sqrt{2\pi}R^{\frac{1}{2}}}\exp\left[-\frac{(y_k - \bar{y}_k)^2}{2R}\right] \tag{39}$$

where y_k signifies the observation vector and $\bar{y}_k$ is the corresponding predicted vector based on prior information.

4.2.3. Results analysis

In this study, the dynamic model of the nonlinear oil dampers is reckoned by the PFMH algorithm. Total 56 sets of the nonlinear oil dampers were put up in the building with eight sets of oil dampers on each floor, four sets of oil dampers in each direction. Two kinds of the dampers with the specification of different stroke limits and orifice are used for 1st floor (Type I) and 3rd to 8th floor (Type II), respectively. To test and quantify the contribution of the oil dampers to the building, both types of dampers are identified using the records mounted on themselves.

The prior distribution for all parameters is on the basis of design, structural drawings and information available in common engineering practice. Then, prior distribution for each parameter is assumed to be independent, and selected as follows: for 1st floor oil damper (Type I), c_d and k_d follow Gaussian distribution with mean $\mu_{k_d} = 1.6$ kN/mm, $\mu_{c_d} = 0.12$ kN · s/mm, additionally, a coefficient of variation is set up to be 20%; parameter α is assigned to be uniform distribution in [0, 1.5]; As for the 8th floor oil dampers (Type II), the parameter k_d, c_d, and α_d are chosen as uniform distribution, i.e. $k_d \sim U(1.5, 2.5), c_d \sim U(0, 0.5), \alpha_d \sim U(0.5, 2)$. The selected prior distributions for every parameter are illustrated as following Fig. 11.

The posterior distribution of identified parameters of the Kelvin-Voigt model are displayed in Fig. 12, additionally, PFMH estimates of the parameters marginal posterior distributions are also shown in Fig. 11. From the observation of identification results, the distributions of parameters k_d, c_d, and α_d are narrow and sharp, which indicate a relatively small variance of each identified parameter. In particular, parameter k_d possesses the least variance. Besides, the posterior distributions of identified parameters also show that the developed PFMH method works well with nonlinear system without stuck to special particles, and is able to circumvent the particle depletion successfully. Moreover, the maximum a posteriori (MAP) estimation is employed to identify the model parameters k_d, c_d, and α_d. Therefore, the MAP estimation of both specifications of the nonlinear oil damper are illustrated for longitudinal orientation (EW) in Table 4.

The comparisons between estimates and corresponding measurements of the damper force time histories and the hysteresis loops of the 1st floor nonlinear oil dampers and 8th floor nonlinear oil dampers are drawn as illustrated in Fig. 13 (a) and (b), respectively. Besides, Normalized root mean squared error (NRMS) is utilized to measure the accuracy for the estimated or predicted response, which can be defined as follows:

$$NRMS = \frac{\|F_\mathrm{d}(t) - \widehat{F}_\mathrm{d}(t)\|}{\|F_\mathrm{d}(t) - mean(F_\mathrm{d}(t))\|} \tag{40}$$

where $\|\bullet\|$ represents the 2-norm function of a vector. $F_\mathrm{d}(t)$ denotes the measured observation vector, $\widehat{F}_\mathrm{d}(t)$ is the corresponding

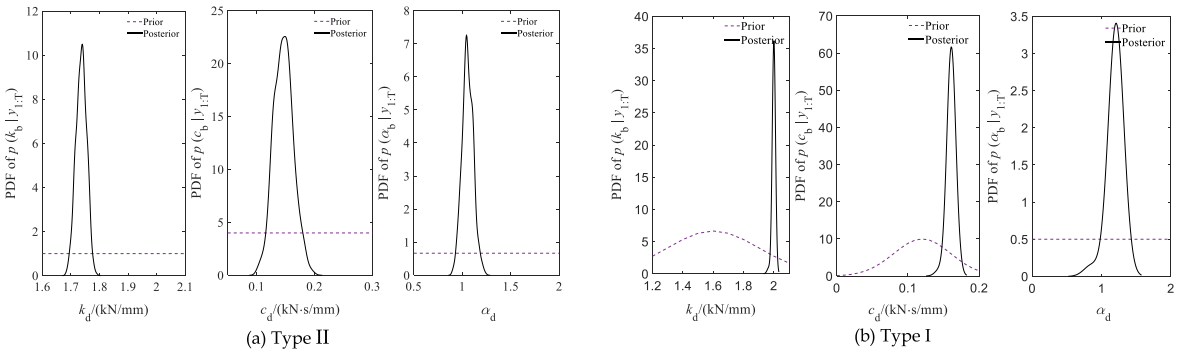

Fig. 11. PFMH estimate of the parameter marginal posterior distributions.

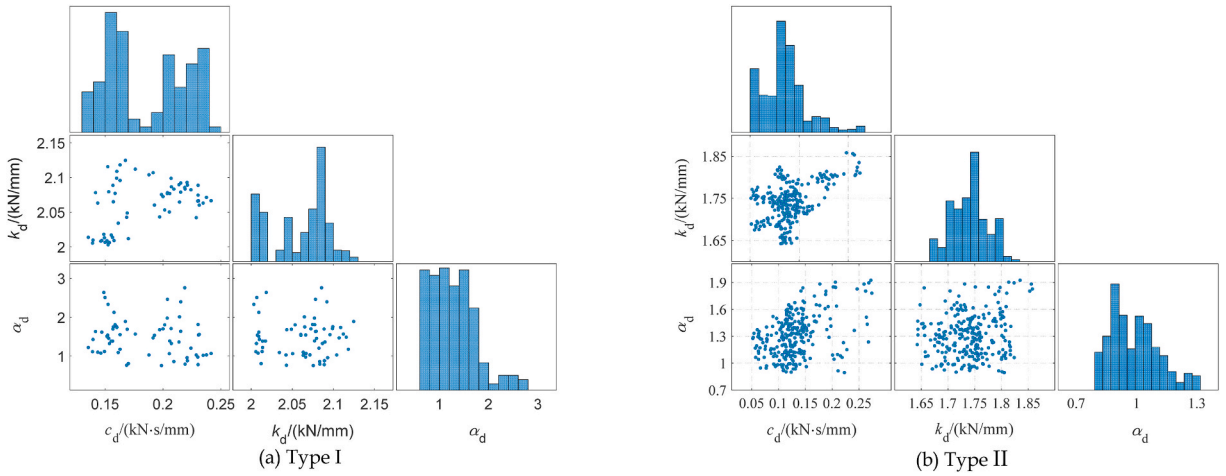

Fig. 12. Identified Kelvin-Voigt model parameter distribution for the nonlinear oil dampers in longitudinal direction (EW).

Table 4
Estimates of model parameters for oil dampers.

Damper type	Kelvin body	C_d (kN•s/mm)	K_d (kN/mm)	α_d
Damper I	Nonlinear	0.23	2.08	1.10
Damper II	Nonlinear	0.12	1.75	1.06

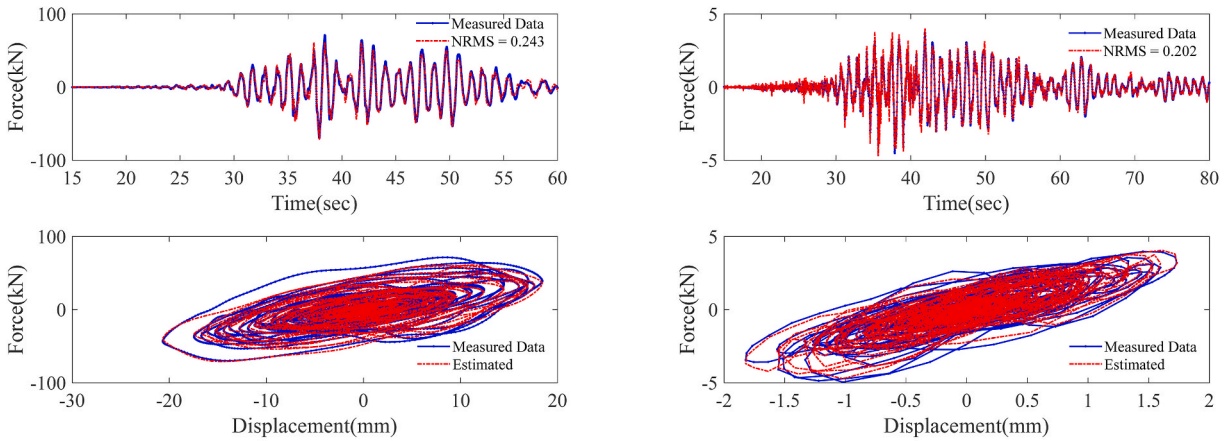

(a) Compare the estimates with records for Type I

(b) Compare the estimates with records for Type II

Fig. 13. Identification or validation results of the nonlinear oil dampers for both Type I and II in longitudinal (EW) orientation.

posterior response estimates of the damper force. Here, the NRMS values vary between -Inf and 1, and the NRMS value approximate to 0 indicates perfect fit with nearly zero error, the other way around represents bad fit.

As can be observed from the identification results in Fig. 13 that the estimated damper responses are pretty consistent with the measurements, the NRMS values are 24.3% and 20.2% for the nonlinear oil damper I and II in longitudinal (EW) directions, respectively. Besides, the estimated hysteretic loops of the relative displacement versus the damper forces are also consistent with that of the recorded inter-story displacement versus the measured damper forces. The satisfactory consistency demonstrates that the Kelvin-Voigt model is able to basically capture the primary dynamic characteristics of the nonlinear oil damper. In addition, both states and parameters of the nonlinear damper model can be effectively identified by the developed PFMH approach, and the PFMH algorithm is robust with regard to different initial distribution.

To further validate the identified nonlinear model and predict the model response of the nonlinear oil damper braces under other earthquakes, recorded data with respect to other three large earthquake records with a moment magnitude more than 7.0 are employed for analysis. The recorded seismic responses on 2005/08/16, 2011/03/09 and 2011/04/07 are exploited to validate the training models which are defined by the posterior parameters identified under May 26th, 2003 earthquake records. As its often the

case that identifying under different excitation signals yields different interpretations of the model, the final identified models are then evaluated by predicting the response of the nonlinear oil damper under the seismic recordings listed in Table 1. The comparison between the measured and predicted responses for nonlinear damper type II in longitudinal (EW) direction are then illustrated as an example in Fig. 14.

4.3. Additional damping ratios provided by oil dampers

To further probe damping characteristics and practical contribution of the nonlinear type of oil damper with viscoelastic polymer packing soft rings, an estimation approach for the equivalent damping ratios offered by the nonlinear oil dampers is presented here. In this research, the modal strain energy method is introduced to reckon the additional damping ratio supplied by the nonlinear oil dampers. First, suppose that a harmonic excitation force with a frequency that's the same as the jth natural frequency of the building is imposed on the building. Second, the building's deformation is proportional to the corresponding mode shape. Thus, the oil damper also vibrates in a harmonic motion, and the equivalent damping ratio of the j th mode provided by oil dampers following the modal strain energy method can be computed as follows:

$$\zeta_{j,d} = \frac{\sum_{n=1}^{n_d} E_{j,n}^{d}}{4\pi E_{S,j}} \tag{41}$$

where $E_{j,n}^{d}$ is the energy dissipation of the nth oil damper under the jth mode in one cycle of motion, and $\sum_{n=1}^{n_d} E_{j,n}^{d}$ then denotes total energy dissipation of all oil dampers under the jth mode in one cycle of motion, n_d is the total number of oil dampers brace, $E_{S,j}$ denotes the maximum strain energy deposited in the entire system under the jth mode in one cycle of motion, and can be calculated by letting the maximum deformation vector of the system in one cycle of motion equal to $\Delta_j = \gamma\varphi_j$, where φ_j denotes the jth mode shape which has been mass-normalized, and γ denotes amplitude factor, then the maximum strain energy deposited in the entire system under the jth mode in one cycle of motion can be presented as follows:

$$E_{S,j} = \frac{1}{2}\Delta_j^T K \Delta_j = \frac{1}{2}\gamma^2 \varphi_j^T K \varphi_j = \frac{1}{2}\gamma^2 \omega_j^2 \tag{42}$$

where K denotes the stiffness matrix and ω_j is the jth fundamental circular frequency of the system.

From this, the corresponding maximum axial deformation between two ends of the nth oil damper brace is calculated as follows:

$$x_{n,\max}^{d} = \gamma\varphi_{j,n} \tag{43}$$

where $\varphi_{j,n}$ is the axial deformation of the nth oil damper brace in the jth mass-normalized mode shape, and the superscript d means damper.

Under the premise of assuming in a harmonic motion, formulate $x_d(t) = x_{n,\max}^{d} \sin(\omega_j t)$ into Equation (19) yields:

$$F_{d,n}(t) = k_{d,n} x_{n,\max}^{d} \sin(\omega_j t) + F_n(t) \tag{44}$$

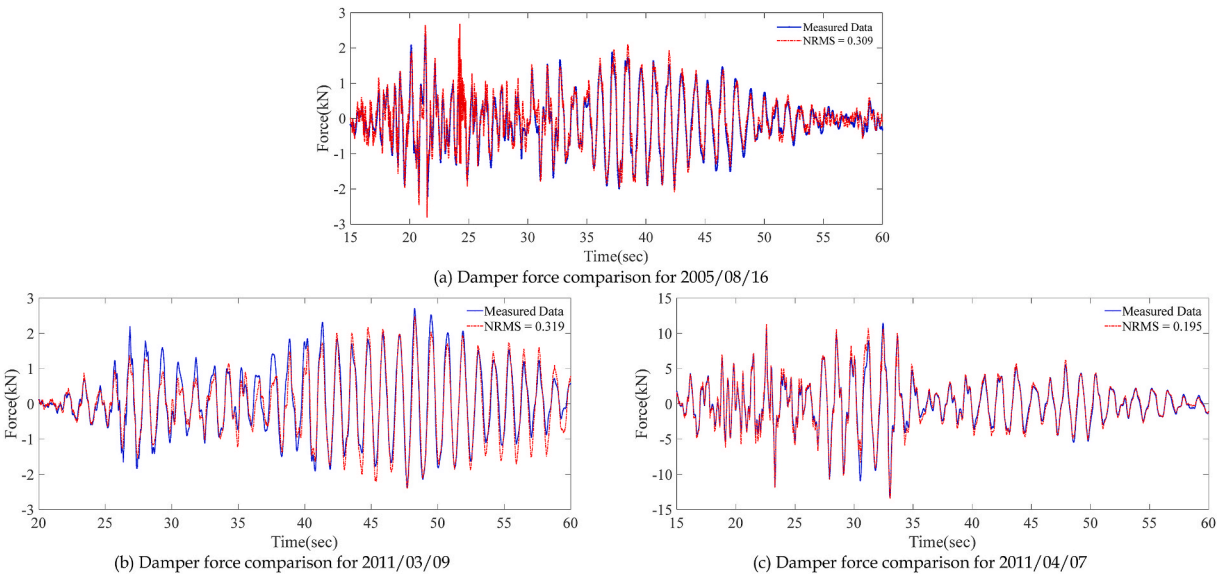

(a) Damper force comparison for 2005/08/16

(b) Damper force comparison for 2011/03/09

(c) Damper force comparison for 2011/04/07

Fig. 14. Model evaluation of the nonlinear oil damper Type II under strong earthquake records in longitudinal (EW) orientation.

where $F_n(t)$ is appointed to the viscous dashpot force imposed on nth oil damper, and is expressed as $F_n(t) = F_{n,\max}\cos(\omega_j t)$. Since the viscous dashpot is the only element for Kelvin-Voigt model which can consume energy, so the energy dissipation $E_{j,n}^d$ could be calculated as follows:

$$E_{j,n}^d = \int_0^{2\pi/\omega_j} F_n(t)\dot{x}_d(t)dt = \int_0^{2\pi/\omega_j} F_n(t)\left(\frac{F_n(t)}{c_{\mathrm{d},n}}\right)^{1/\alpha_n} dt \tag{45}$$

where $\dot{x}_d(t)$ is the velocity of the nth nonlinear oil damper brace, $c_{\mathrm{d},n}$ and α_n are assigned as the damping coefficients and exponent coefficient of velocity of viscous dashpot of the nth oil damper brace, respectively. The solution for Equation (45) can be obtained analytically, that is

$$E_{j,n}^d = 2\sqrt{\pi}\,\frac{\Gamma\left(1+\frac{1}{2\alpha_n}\right)}{\Gamma\left(\frac{3}{2}+\frac{1}{2\alpha_n}\right)}\,\frac{F_{n,\max}^{1+1/\alpha_n} c_{\mathrm{d},n}^{-1/\alpha_n}}{\omega_j} \tag{46}$$

in which Γ denotes the gamma function. Moreover, from Kelvin-Voigt model Equation (19), $F_{n,\max}$ equals to $F_{n,\max} = c_{\mathrm{d},n}\omega_j^{\alpha_n}\left(x_{\mathrm{n},\max}^d\right)^{\alpha_n}$ under the jth mode in one cycle of motion.

Substituting Equations (42) and (46) into Equation (41) yields

$$\zeta_{j,d} = \frac{\sum_{n=1}^{n_d}\frac{\Gamma\left(1+\frac{1}{2\alpha_n}\right)}{\Gamma\left(\frac{3}{2}+\frac{1}{2\alpha_n}\right)} c_{\mathrm{d,n}}\left(\omega_j\gamma\varphi_{j,n}\right)^{\alpha_n+1}}{\sqrt{\pi}\gamma^2\omega_j^3} \tag{47}$$

As the viscosity coefficients $c_{\mathrm{d,n}}$ and the velocity exponent coefficients, α_n for all nonlinear oil dampers were determined by PFMH, and the significant modes were also available in section 3.2. Thus, the supplemental damping ratios supplied by viscous damper braces can be estimated following above approach by Equation (47). Since the specification, total number, and allocation of the nonlinear oil dampers in transverse orientation (NS) are the same with the longitudinal orientation (EW), the supplemental equivalent damping ratios in the longitude (EW) orientation for strong earthquake records are estimated and listed in Table 5.

From the results in Table 5, additional equivalent damping ratios of the nonlinear oil damper brace for the 1st and 2nd mode are around 1% and 2%, respectively. While the estimated additional equivalent damping ratio varies significantly for the 3rd mode. Since oil dampers were damaged for the 1st floor and had severe oil leakages for the third and fourth floors during Great Japan earthquake on Mar 11th, 2011, the estimated additional equivalent damping ratios of recording 2011/04/07 are quite small for the 1st and 2nd mode. At the same time, the structural seismic responses of recording 2011/04/07 were the largest among the recorded four strong earthquakes, which indicated that the nonlinear oil damper braces effectively mitigate seismic vibration of the steel building. The additional equivalent damping ratio contribution of the nonlinear oil dampers on each floor is illustrated in Fig. 15.

As can be observed from the results in Fig. 15, the equivalent damping ratio offered by oil dampers on first floor contributes to most of the total additional equivalent damping ratio, while the oil dampers on other floors (3F–8F) account for a smaller proportion. Among them, the oil dampers on first floor account for more than 77% of the 1st mode additional equivalent damping ratio, and more than 58% of the 2nd mode additional equivalent damping ratio. This is mainly due to the large inter-story deformation of the first floor and the high energy consumption of the nonlinear oil dampers on the first floor. For the first-order effective damping ratio contribution, the proportion of the oil damper gradually decreases with the increase of the floor, while in the second and third-order effective damping ratio contributions, the proportion of the high floor increases significantly. Nevertheless, due to the second-order and third-order modal responses are relatively small, and the damping energy consumption of the high-floor oil damper is limited, the oil dampers on high floors have less significant effect on the seismic response of the steel building.

5. Conclusions

This paper investigates a type of nonlinear oil damper with viscoelastic materials implemented to an eight-story passively-controlled steel building. The instrumented steel building has experienced over 21 earthquakes since it was built in 2003 including four intense earthquake records with a moment magnitude more than 7.0. System identification was exploited to the recorded actual earthquake responses to extract dynamic properties of the whole building. Besides, parameters of the nonlinear oil damper model were identified. Furthermore, a simplified estimation procedure of equivalent damping ratios provided by the nonlinear oil dampers is proposed, and calculation formulas of the additional damping ratio provided by oil dampers are deduced using modal strain energy.

From the identified dynamic characteristics of the passively-controlled eight-story steel building, natural frequencies for recording 2003/5/26, 2005/8/16 and 2011/3/9 are stable over the eight-year period studied, so are the first two damping ratio, which indicates that the global dynamic properties had no significant change for the steel building during this period before 3•11 earthquake. Nevertheless, the identified first two fundamental frequency and damping ratio decrease significantly for recording 2011/4/7, which laid on two main reasons: first, the connections and non-structural elements may undergo some micro damage which can't be inspected by visual; second, the decrease of both frequency and damping ratio indicates that the oil damper braces not only provide supplemental damping, but also offer additional stiffness to the steel building.

The parameter identification results also reveal that Kelvin-Voigt model basically captures the primary dynamic characteristics of

Table 5
Equivalent damping ratio of oil damper braces by Kelvin-Voigt model.

	Mode	2003/05/26	2005/08/16	2011/03/09	2011/04/07
$\zeta_{j,d}$ (%)	1st mode	0.96	1.18	1.17	0.14
	2nd mode	1.91	2.14	2.28	0.83
	3rd mode	1.45	6.01	0.85	1.02

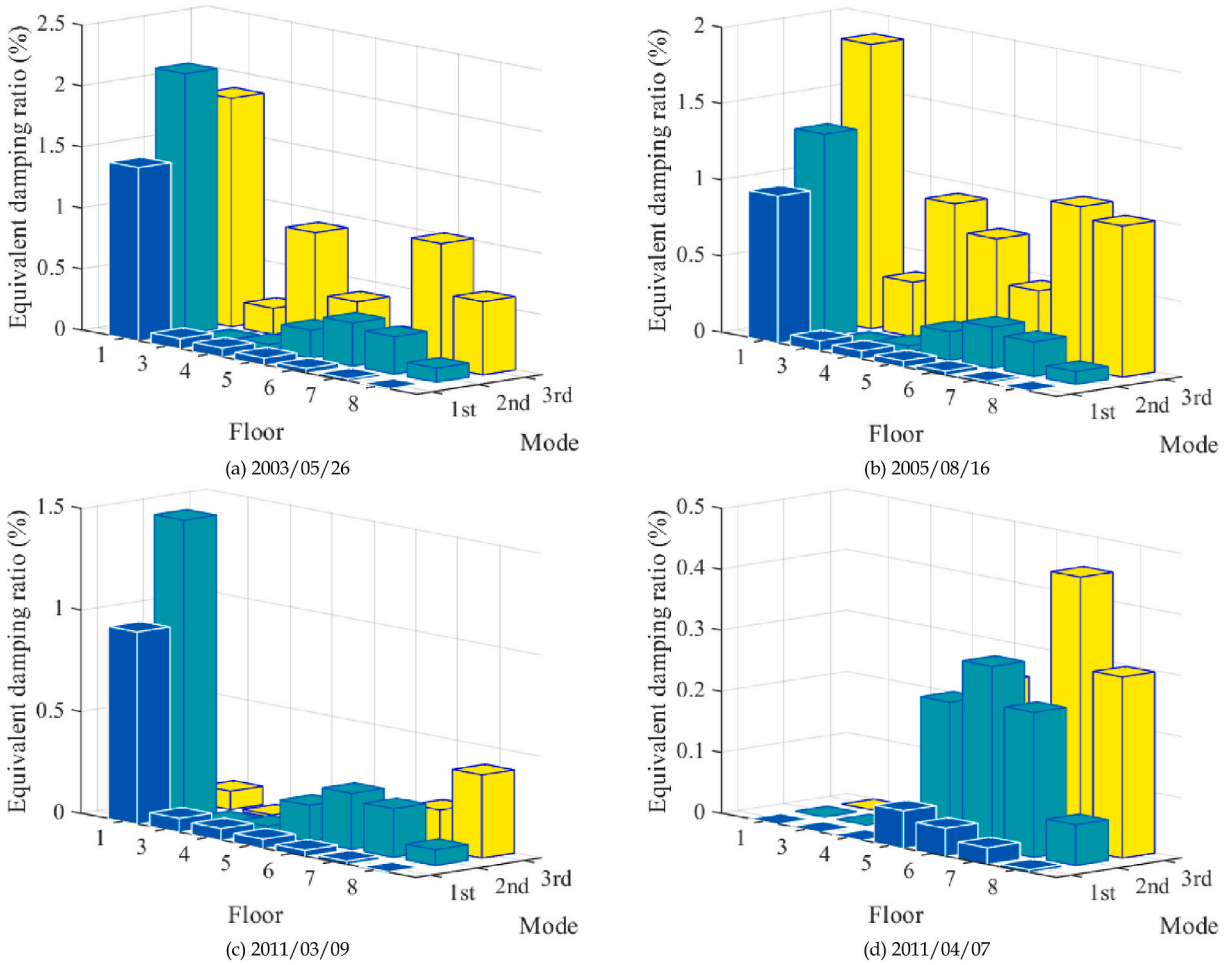

Fig. 15. The additional equivalent damping ratio contribution of the nonlinear oil damper braces on each floor.

the nonlinear oil damper. In addition, both states and parameters of the nonlinear damper model can be effectively identified by the improved PFMH approach through state augmentation in this case. Nevertheless, although the PFMH algorithm is robust with regard to different initial condition, the augmented state approach may aggravate the sample impoverishment problem for even higher dimension parameter identification.

The estimated effective damping ratio of oil damper presented in this paper shows that additional equivalent damping ratios of the nonlinear oil damper brace for the 1st and 2nd mode are around 1% and 2%, respectively. Besides, the equivalent damping ratio offered by oil dampers on first floor contributes to most of the total additional equivalent damping ratio due to the large inter-story deformation of the first floor and the high energy consumption of the nonlinear oil dampers on the first floor. As the oil dampers on other floors (5F–8F) account for an even smaller proportion, the first-order damping ratio of main frame of the steel building is approximately 0.017.

Author statement

Yunjia Tong (First Author): Conceptualization, Methodology, Software, Investigation, Formal Analysis, Writing - Original Draft; Songtao Xue: Data Curation, Visualization, Investigation; Liyu Xie (Corresponding Author):Conceptualization, Funding Acquisition, Resources, Supervision, Writing - Review & Editing, Hesheng Tang: Validation.

Declaration of competing interest

The authors declare that they have no known competing financial interests or personal relationships that could have appeared to influence the work reported in this paper.

Data availability

Data will be made available on request.

Acknowledgements

The authors express their sincere thanks to the research team who conducted the structural health monitoring of a passively controlled eight-story steel building with various types of dampers (Leader: Professor Songtao Xue, Tongji University and Tohoku Institute of Technology). The authors also acknowledge the financial support from Funds National Natural Science Foundation of China (Grant No. 2021YFE0112200), the Natural Science Foundation of Shanghai (Grant No. 20ZR1461800), and the Tohoku Institute of Technology research Grant. The findings in this paper are those of the authors and do not necessary reflect the view of the sponsors.

References

[1] C. Christopoulos, A. Filiatrault, V.V. Bertero, Principles of Passive Supplemental Damping and Seismic Isolation, vol. 133, Iuss press Pavia, Italy, 2006.
[2] X. Ji, et al., Damping identification of a full-scale passively controlled five-story steel building structure, Earthq. Eng. Struct. Dynam. 42 (2) (2013) 277–295.
[3] M.C. Constantinou, et al., Toggle-brace-damper seismic energy dissipation systems, J. Struct. Eng. 127 (2) (2001) 105–112.
[4] Y.T. Chen, Y.H. Chai, Seismic Design of Structures with Supplemental Maxwell Model-Based Brace-Damper Systems, 2008.
[5] C. Lee, et al., Optimal design theories and applications of tuned mass dampers, Eng. Struct. 28 (1) (2006) 43–53.
[6] T.T. Soong, B.F. Spencer Jr., Supplemental energy dissipation: state-of-the-art and state-of-the-practice, Eng. Struct. 24 (3) (2002) 243–259.
[7] T.T. Soong, G.F. Dargush, * Passive Energy Dissipation Systems in Structural Engineering, Wiley, 1997.
[8] K. Kasai, et al., Performance of seismic protection technologies during the 2011 Tohoku-Oki earthquake, Earthq. Spectra 29 (1_suppl) (2013) 265–293.
[9] N.K. Hazaveh, et al., Experimental test and validation of a direction-and displacement-dependent viscous damper, J. Eng. Mech. 143 (11) (2017), 04017132.
[10] R. Greco, G.C. Marano, Identification of parameters of Maxwell and Kelvin–Voigt generalized models for fluid viscous dampers, J. Vib. Control 21 (2) (2015) 260–274.
[11] K. Kasai, et al., Full Scale Shake Table Tests of 5-story Steel Building with Various Dampers, 2010.
[12] J. Hwang, et al., Experimental study of RC building structures with supplemental viscous dampers and lightly reinforced walls, Eng. Struct. 28 (13) (2006) 1816–1824.
[13] D. Konstantinidis, N. Makris, J.M. Kelly, Health monitoring of fluid dampers for vibration control of structures: experimental investigation, Earthq. Eng. Struct. Dynam. 41 (13) (2012) 1813–1829.
[14] A.R. Bixio, et al., Repeatable dynamic release tests on a base-isolated building, J. Earthq. Eng. 5 (2001) 369–393, 03.
[15] Y.T. Chen, Y.H. Chai, Effects of brace stiffness on performance of structures with supplemental Maxwell model-based brace–damper systems, Earthq. Eng. Struct. Dynam. 40 (1) (2011) 75–92.
[16] K.C. Chang, et al., Seismic behavior of steel frame with added viscoelastic dampers, J. Struct. Eng. 121 (10) (1995) 1418–1426.
[17] M.C. Constantinou, M.D. Symans, Experimental study of seismic response of buildings with supplemental fluid dampers, Struct. Des. Tall Build. 2 (2) (1993) 93–132.
[18] K. Chang, Y. Lin, Seismic response of full-scale structure with added viscoelastic dampers, J. Struct. Eng. 130 (4) (2004) 600–608.
[19] D. De Domenico, G. Ricciardi, Earthquake protection of structures with nonlinear viscous dampers optimized through an energy-based stochastic approach, Eng. Struct. 179 (2019) 523–539.
[20] S. Akcelyan, D.G. Lignos, T. Hikino, Adaptive numerical method algorithms for nonlinear viscous and bilinear oil damper models subjected to dynamic loading, Soil Dynam. Earthq. Eng. 113 (2018) 488–502.
[21] C. Li, et al., Equivalent damping of SDOF structure with Maxwell damper, Earthq. Eng. Eng. Vib. 17 (3) (2018) 627–639.
[22] X. Jiao, Y. Zhao, W. Ma, Nonlinear dynamic characteristics of a micro-vibration fluid viscous damper, Nonlinear Dynam. 92 (3) (2018) 1167–1184.
[23] Y. Liu, J. Wu, M. Donà, Effectiveness of fluid-viscous dampers for improved seismic performance of inter-storey isolated buildings, Eng. Struct. 169 (2018) 276–292.
[24] A. Bajrić, J. Høgsberg, Identification of damping and complex modes in structural vibrations, J. Sound Vib. 431 (2018) 367–389.
[25] N. Pollini, O. Lavan, O. Amir, Minimum-cost Optimization of Nonlinear Fluid Viscous Dampers and Their Supporting Members for Seismic Retrofitting, Earthquake Engineering & Structural Dynamics, 2017.
[26] R. Lewandowski, M. Łasecka-Plura, Design sensitivity analysis of structures with viscoelastic dampers, Comput. Struct. 164 (2016) 95–107.
[27] A. Ras, N. Boumechra, Seismic energy dissipation study of linear fluid viscous dampers in steel structure design, Alex. Eng. J. 55 (3) (2016) 2821–2832.
[28] S. Matsuda, Optimum Design of Maxwell-type Damper System Based on Stochastically Equivalent Damping Factor, 2012.
[29] B. Dong, R. Sause, J.M. Ricles, Accurate real-time hybrid earthquake simulations on large-scale MDOF steel structure with nonlinear viscous dampers, Earthq. Eng. Struct. Dynam. 44 (12) (2015) 2035–2055.
[30] S. Kawamata, N. Funaki, Y. Itoh, Passive Control of Building Frames by Means of Liquid Dampers Sealed by Viscoelastic Material, in 12th World Conference on Earthquake Engineering, 2000.
[31] K. Worden, J.J. Hensman, Parameter estimation and model selection for a class of hysteretic systems using Bayesian inference, Mech. Syst. Signal Process. 32 (2012) 153–169.
[32] T. Saito, J.L. Beck, Bayesian model selection for ARX models and its application to structural health monitoring, Earthq. Eng. Struct. Dynam. 39 (15) (2010) 1737–1759.
[33] S.H. Cheung, Stochastic Analysis, Model and Reliability Updating of Complex Systems with Applications to Structural Dynamics, 2009.
[34] T. Rainforth, et al., Interacting Particle Markov Chain Monte Carlo, in International Conference on Machine Learning, 2016 (PMLR).
[35] C. Andrieu, A. Doucet, R. Holenstein, Particle Markov chain Monte Carlo methods, J. Roy. Stat. Soc. B 72 (3) (2010) 269–342.
[36] N. Gordon, Beyond the Kalman Filter: Particle Filters for Tracking Applications, 2004.
[37] M. Cao, et al., Performance study of an 8-story steel building equipped with oil damper damaged during the 2011 Great East Japan earthquakePart 2: nonlinear retrofit strategy, J. Asian Architect. Build Eng. 15 (2) (2018) 303–310.
[38] E. Reynders, System identification methods for (operational) modal analysis: review and comparison, Arch. Comput. Methods Eng. 19 (1) (2012) 51–124.
[39] Y. Minami, S. Yoshitomi, I. Takewaki, System identification of super high-rise buildings using limited vibration data during the 2011 Tohoku (Japan) earthquake, Struct. Control Health Monit. 20 (11) (2013) 1317–1338.
[40] X. Ji, et al., Seismic damage detection of a full-scale shaking table test structure, J. Struct. Eng. 137 (1) (2011) 14–21.

[41] S.Y. Chu, S.C. Lo, Application of the on-line recursive least-squares method to perform structural damage assessment, Struct. Control Health Monit. 18 (3) (2011) 241–264.
[42] S.N. Pakzad, G.L. Fenves, Statistical analysis of vibration modes of a suspension bridge using spatially dense wireless sensor network, J. Struct. Eng. 135 (7) (2009) 863–872.
[43] T. Saito, System Identification of a High-Rise Building Applying Multi-Input-Multi-Output ARX Model of Modal Analysis; Mode Kaisekigata Tanyuryoku Tashutsuryoku ARX Model Wo Mochiita Koso Kenbutsu No System Dotei, Nippon Kenchiku Gakkai Kozo-kei Ronbunshu, 1998.
[44] M. Muto, J.L. Beck, Bayesian updating and model class selection for hysteretic structural models using stochastic simulation, J. Vib. Control 14 (1–2) (2008) 7–34.
[45] J.L. Beck, Probability logic, information quantification and robust predictive system analysis, EERL Report (2008) 17–22, 2008-05.
[46] J.L. Beck, K. Yuen, Model selection using response measurements: Bayesian probabilistic approach, J. Eng. Mech. 130 (2) (2004) 192–203.
[47] J.L. Beck, L.S. Katafygiotis, Updating models and their uncertainties. I: Bayesian statistical framework, J. Eng. Mech. 124 (4) (1998) 455–461.
[48] E. Şafak, Adaptive modeling, identification, and control of dynamic structural systems. I: Theory, J. Eng. Mech. 115 (11) (1989) 2386–2405.
[49] E. Şafak, Adaptive modeling, identification, and control of dynamic structural systems. II: applications, J. Eng. Mech. 115 (11) (1989) 2406–2426.
[50] D.M. Siringoringo, Y. Fujino, Seismic response analyses of an asymmetric base-isolated building during the 2011 Great East Japan (Tohoku) Earthquake, Struct. Control Health Monit. 22 (1) (2015) 71–90.
[51] R.S. Pappa, K.B. Elliott, A. Schenk, Consistent-mode indicator for the eigensystem realization algorithm, J. Guid. Control Dynam. 16 (5) (1993) 852–858.
[52] N. Funaki, J. Kang, S. Kawamata, Vibration Response of a Three-Storied Full-Scale Test Building Passively Controlled by Liquid Dampers Sealed by Viscoelastic Material, 12th World Conference on Earthquake Engineering, 2001.
[53] S. Kawamata, N. Funaki, Y. Itoh, Passive Control of Building Frames by Means of Liquid Dampers Sealed by Viscoelastic Material, 12th World Conference on Earthquake Engineering, 2000.
[54] I. López, J.M. Busturia, H. Nijmeijer, Energy dissipation of a friction damper, J. Sound Vib. 278 (3) (2004) 539–561.
[55] J.S. Liu, Monte Carlo Strategies in Scientific Computing, Springer Science & Business Media, 2008.
[56] F.E. Daum, J. Huang, Dynamic Quasi-Monte Carlo for Nonlinear Filters, International Society for Optics and Photonics, 2003.
[57] F. Daum, J. Huang, Curse of Dimensionality and Particle Filters, IEEE, 2003.
[58] C. Snyder, T. Bengtsson, M. Morzfeld, Performance bounds for particle filters using the optimal proposal, Mon. Weather Rev. 143 (11) (2015) 4750–4761.
[59] C. Snyder, et al., Obstacles to high-dimensional particle filtering, Mon. Weather Rev. 136 (12) (2008) 4629–4640.
[60] J.S. Liu, R. Chen, Sequential Monte Carlo methods for dynamic systems, J. Am. Stat. Assoc. 93 (443) (1998) 1032–1044.
[61] M.S. Arulampalam, et al., A tutorial on particle filters for online nonlinear/non-Gaussian Bayesian tracking, IEEE Trans. Signal Process. 50 (2) (2002) 174–188.
[62] R. Rocchetta, et al., On-line Bayesian model updating for structural health monitoring, Mech. Syst. Signal Process. 103 (2018) 174–195.
[63] J. Liu, M. West, Combined Parameter and State Estimation in Simulation-Based Filtering, Springer, 2001, pp. 197–223.
[64] T.C. Clapp, Statistical Methods for the Processing of Communications Data, University of Cambridge, 2001.
[65] O. Cappé, S.J. Godsill, E. Moulines, An overview of existing methods and recent advances in sequential Monte Carlo, Proc. IEEE 95 (5) (2007) 899–924.
[66] B. Ristic, S. Arulampalam, N. Gordon, Beyond the Kalman Filter: Particle Filters for Tracking Applications, Artech house, 2003.
[67] C. Andrieu, A. Doucet, Particle filtering for partially observed Gaussian state space models, J. Roy. Stat. Soc. B Stat. Methodol. 64 (4) (2002) 827–836.
[68] A. Gelman, W.R. Gilks, G.O. Roberts, Weak convergence and optimal scaling of random walk Metropolis algorithms, Ann. Appl. Probab. 7 (1) (1997) 110–120.
[69] D. Sivia, J. Skilling, Data Analysis: a Bayesian Tutorial, OUP, Oxford, 2006.